Journal of Molecular Graphics and Modelling 38 (2012) 13–25

Contents lists available at SciVerse ScienceDirect

Journal of Molecular Graphics and Modelling

journal homepage: www.elsevier.com/locate/JMGM

Preferential heterochiral cyclic trimerization of 5-(aminoethyl)-2-furancarboxylic acid (AEFC) driven by non-covalent interactions

N.V. Suresh Kumar[a], Harjinder Singh[a,*], Kiran Kumar Pulukuri[b], Tushar Kanti Chakraborty[b]

[a] International Institute of Information Technology-Hyderabad, Hyderabad 500032, India
[b] Central Drug Research Institute, Lucknow 226 001, India

ARTICLE INFO

Article history:
Accepted 5 May 2012
Available online 12 June 2012

Keywords:
Homo/heterochiral
DFT
Microsolvation
NBO
AIM
MESP

ABSTRACT

Theoretical justification for preferential heterochiral cyclic trimerization of 5-(aminoethyl)-2-furancarboxylic acid (AEFC) is attempted using density functional theory (DFT) calculations. Results from explicit solvent assisted reaction pathways indicate greater stability of heterochiral cyclic tripeptides over their homochiral counterparts, contrary to findings from gas phase and implicit solvent phase results. Pathways explored at M06/6-31G(d,p) and MP2/6-31G(d,p) levels of theory show kinetic preference for heterochiral cyclization. Analysis of optimized geometries reveals existence of strong hydrogen bonding interactions in the solvated heterochiral tripeptides. Thus, the ability of the cyclic tripeptides to form strong noncovalent interactions increases with conversion of stereochemistry at one of its chiral centers from homo to heterochiral conformation. The resulting change in molecular symmetry facilitates the interacting sites to reorient such that the peptide can interact with a nucleophile from both the faces. This is further substantiated by computed IR spectra, NBO and AIM data. Additionally, justification for the stability of heterochiral cyclic tripeptides comes from molecular electrostatic potential and electron density surfaces. These studies show clearly that for the kind of systems presented here, gas phase or implicit solvent phase studies are inadequate in explaining realistic situations. Calculations with solvent molecules, even if a few only, are necessary to substantiate experimental observations.

1. Introduction

Theoretical studies on molecular structure and properties of cyclic peptides are imperative to understand diverse reactive features in such systems. Many such systems are known to have enhanced biological properties, as compared to their linear analogs [1], due to their restricted conformational flexibility. Cyclization of linear peptides has become a widely used method to induce desirable structural biases essential for biological activities [2–7]. Cyclic peptides with rigid molecular frameworks, notably those formed by unnatural amino acids [8], containing predisposed cavities of precise dimensions are attractive tools to carry out in vitro studies on molecular recognition processes [6]. Synthetic receptors with specific recognition properties for anions are important candidates in supramolecular chemistry [9–14], many of them containing multidentate H-bonding sites [15,16].

Recently, Chakraborty et al. have reported that 5-(aminomethyl)-2-furan carboxylic acid (AMFC) based cationic cyclic homo-oligopeptides are efficient G-quadruplex binders [17,18]. They have also synthesized a novel cyclic tripeptide, from an optically active monomer building block 5-(aminoethyl)-2-furan carboxylic acid (AEFC) in the solvent N,N,-dimethyl-formamide (DMF) [6]. The homochiral cyclic tripeptide formed by AEFC is studied for anion binding, antimicrobial properties and reported to show significant activities against some Gram-positive and Gram-negative bacteria [6]. It is known that for anion recognition, amide groups in cyclic peptides, with ability to form H-bonds play a vital role [9,16]. Selective binding relies on structure and intrinsic ability to form noncovalent interactions. Chirality has important role in molecular architecture and functionality [19,20]. We have envisaged that change in stereochemistry at one chiral center will alter nature of interactions shown by the peptide.

In the present work, we model isolated and solvent assisted linear and cyclic peptides formed by the molecule. An important observation is that nature of noncovalent interactions, in explicit solvent (DMF) phase, change significantly upon conversion of

* Corresponding author. Tel.: +91 4066531277; fax: +91 4066531413.
E-mail addresses: harjinder.singh@iiit.ac.in, laltu@iiit.ac.in (H. Singh).

1093-3263/$ – see front matter © 2012 Elsevier Inc. All rights reserved.
http://dx.doi.org/10.1016/j.jmgm.2012.05.010

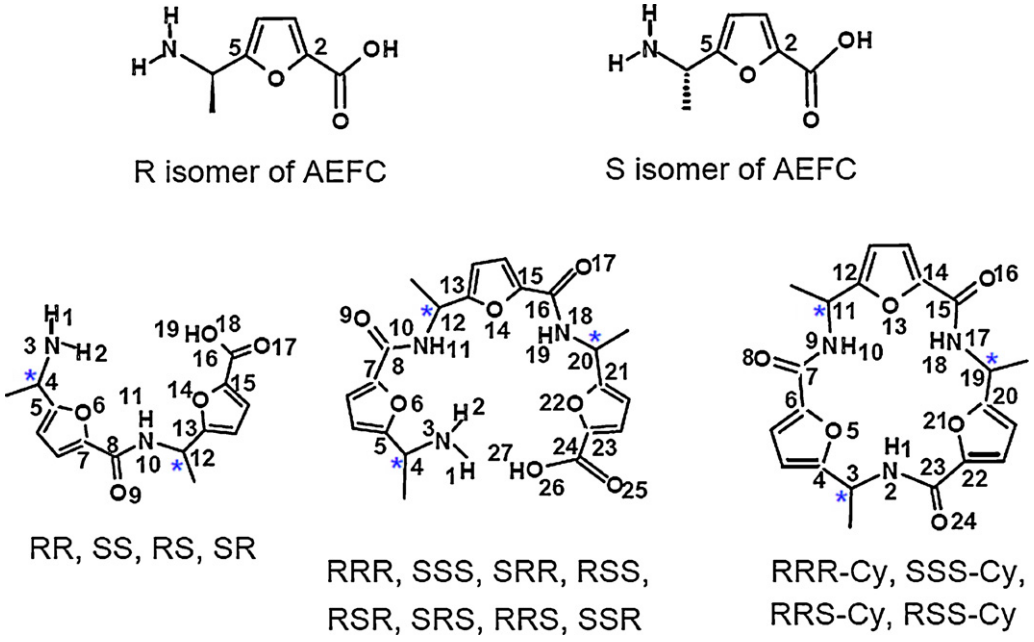

Fig. 1. Schematic representation of R-5-(aminoethyl)-2-furancarboxylic acid, **R-AEFC**, and S-5-(aminoethyl)-2-furancarboxylic acid, **S- AEFC** (conventional atom numbering is used for furan ring); linear dipeptides, **RR**, **SS**, **RS** and **SR**; linear tripeptides **RRR**, **SSS**, **SRR**, **RSS**, **RSR**, **SRS**, **RRS**, and **SSR**; and cyclic tripeptides **RRR-Cy**, **SSS-Cy**, **RRS-Cy** and **RSS-Cy**. Atom numbering scheme for linear and cyclic peptides shown here is used in the text. ⁎ : chiral center. Linear di and tripeptides are denoted with stereochemistry of amino acids arranged in the order of N- to C-terminal direction in the respective peptide.

stereochemistry at one chiral center. Also, yield of cyclic tripeptide containing two R- and one S-isomers of AEFC (heterochiral form) is higher as compared to that of tripeptide composed of three homo isomeric forms of AEFC. This is contrary to that seen in the gas phase.

Structures and reaction energies of linear di- and tripeptides, and cyclic tripeptides are determined in both gas phase as well as solvent phase. Schematic representation of the structures studied here is shown in Fig. 1. The aim is to gain insights into: (i) chiral preference in the formation of tripeptides, (ii) thermodynamic and kinetic aspects of solvent assisted cyclization of linear tripeptides, and (iii) role of non-covalent interactions in stabilization of the peptides. Reaction pathways leading to cyclic trimerization of linear tripeptides are modeled using simple uncatalyzed straightforward mechanisms investigated by Oie et al. [21] and Jensen et al. [22], shown in Fig. 2(a). The mechanisms are associated with elimination of water molecule(s). They have studied the mechanism using two different models: (i) Stepwise pathway, where one of the hydrogen atoms of the $-NH_2$ group is shifted to the oxygen of C=O resulting in a diol intermediate. The second step involves elimination of water forming the peptide bond; (ii) Concerted pathway involves direct elimination of water molecule, using the —OH from the carboxyl terminal and —H of amine group. Reaction mechanism for the reverse process, i.e., amide hydrolysis via concerted and stepwise mechanisms is also investigated by Krug et al. [23] and by Antonczak et al. [24].

The R- and S-isomers of AEFC are referred to as **R-AEFC** and **S-AEFC**, respectively. Linear di and tripeptides are denoted with stereochemistry of amino acids arranged in the order of N- to C-terminal direction. The notations are shown in Fig. 1. Wherever further discrimination is not required, oligo-peptides composed of homo isomeric forms of the amino acid are called homochiral peptides and the others are referred to as heterochiral peptides. Line drawing pictures of geometries in the reaction pathways and the notation used to name them are shown in Fig. 2(b) and (c). Figures and tables labeled by 'Sn' are shown in supporting information.

2. Computational details and modeling

Initial coordinates for geometries of **R**-, **S-AEFC**, linear di and tripeptides were generated using GaussView [25]. One dimensional potential energy surface of each dipeptide was explored by employing a systematic conformational search with respect to N10—C12 bond (See Fig. 1), at 10° increments over the entire 360° angular space. The search was carried out at HF/6-31G(d,p) [26] level of theory. Minimum energy structure for each dipeptide was identified.

Conformational space of each linear tripeptide was investigated, using random search method provided by Sybyl7.2 [27]. The method samples the space by making random changes to select torsion angles followed by energy minimization [28]. We allowed for rotation about N—C_δ (Cδ: carbon atom at chiral center) bonds, (excluding the bond at N-terminal) (See Fig. 1). The random search parameters were set to default values except that chirality check was turned on. The search generated of the order of 100 initial conformations for each linear tripeptide except for **SRR** and **RSS** (26 and 53, respectively). The conformations within 2 kcal/mol from the lowest energy geometry were subjected to single point energy calculations at B3LYP [29–31]/6-31G(d,p) level of density functional theory (DFT) [32]. Minimum energy structures of linear di and tripeptides were further optimized at B3LYP/6-31G(d,p) level of theory in gas phase.

Initial coordinates of 18 membered cyclic tripeptide, **RRR-Cy** and **SSS-Cy** were obtained from those available in our earlier work on AMFC [8,33,34]. One of the hydrogen atoms at C_δ position of cyclic tripeptide formed by AMFC was replaced by methyl group in such a way that it was in *s-trans* orientation with respect to furan ring. Stereochemistry of the amino acids in the tripeptides was altered so that initial coordinates of other cyclic structures, **RRS-Cy** and **RSS-Cy** could be obtained. The geometries were subjected to optimization at the same level of density functional theory in gas phase.

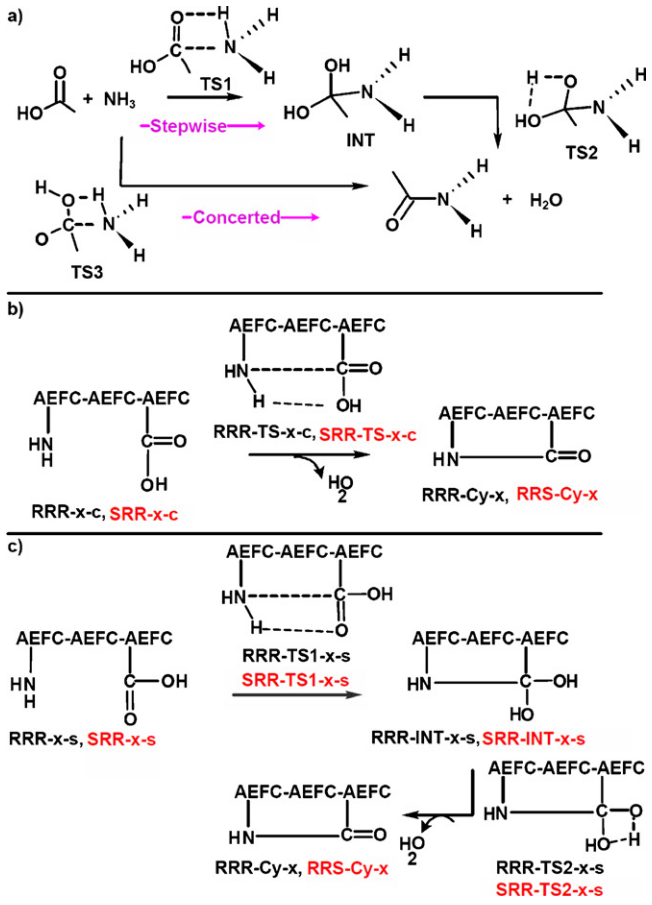

Fig. 2. (a) Uncatalyzed stepwise and concerted mechanisms suggested in the literature for peptide bond formation. Line drawings for structures in (b) concerted and (c) stepwise cyclic trimerization reactions of linear tripeptides formed by R- and S-isomers of AEFC. Representation of symbols used in notation is as follows: **R**, R-AEFC; **S**, S-AEFC; **x** ≡ 2DMF (2 units of DMF molecules); **c**, concerted; **s**, stepwise; **TS**, transition state; **TS1-2**, transition state 1, 2; **Cy**, cyclized. Solvent assisted linear tripeptides, transition states (TSs), intermediates (INT) are denoted with stereochemistry of amino acids arranged in the order of N- to C-terminal direction in the respective peptide. The notation used in text is as indicated here.

All the gas phase optimized geometries were further subjected to optimization in the solvent, DMF, at B3LYP/6-31G(d,p) level of theory using implicit solvent models, 'Onsager reaction field model' [35–37] and polarized continuum model (PCM) [38] of Self Consistent Reaction Field (SCRF) [39] method. The PCM model that uses van der Waals radii for spherical cavities around the atoms (including H), evaluated in the frame of universal force field (UFF) [40] was employed in the present work. Additional microsolvation studies are described below in the next subsection.

Hessian calculations were carried out on the geometries of gas and solvent phases, at the level of theory used for optimization. All geometries show real frequencies indicating that they are at local minimum on potential energy surface. Changes in zero point corrected electronic energy (ΔE) and free energy (ΔG) for formation of products were calculated. The break up of ΔG in terms of enthalpy and entropy was employed to gain insights into role of the thermodynamic parameters in driving the species to lower free energy state.

2.1. Microsolvation studies

Microsolvation of cyclic tripeptides, **RRR-Cy** and **RRS-Cy** was carried out to determine atomic level interactions between solvent (DMF) and solute. The cyclic peptides complexed with '*n*' number of solvent molecules ($n = 1, 2$) were modeled. For $n = 1$, one DMF molecule was placed on three fold axis of rotation of the peptides so that carbonyl oxygen of solvent molecule forms H-bonding interactions with the peptide geometries. Similarly, for $n = 2$, two solvent molecules were placed, one above and another below the plane of cyclic tripeptides and lying on three fold axis of rotation for the peptides. Two conformations (**Con I, II**) were considered for each doubly solvated structure. While in **Con I**, the carbonyl oxygen atoms of both the solvent molecules are oriented towards amide groups of the peptides, in **Con II** the carbonyl oxygen of one of the solvent molecules is pointing towards the NH groups and the other one is directed away from the groups. The selected orientations of solvent molecules examine the ability of the peptides to form strong intermolecular H-bond interactions. The positions chosen are the sites where the orientation of interacting groups in cyclic peptides is distinct. All solvated structures were optimized and further subjected to Hessian calculations at B3LYP/6-31G(d,p) level of theory in gas phase as well as solvent phase using the PCM model. Electronic energies of interaction without and with BSSE (Basis Set Superposition Error) correction and zero point energy (ZPE) correction, i.e., E_{1-int}, E_{2-int} and E_{3-int}, respectively were calculated using the equations.

$$E_{1-int} = E_{X-S_n} - (E_X + nE_S) \quad (1)$$

$$E_{2-int} = (E_{X-S_n} - (E_X + nE_S)) + E_{BSSE} \quad (2)$$

$$E_{3-int} = E^Z_{X-S_n} - (E^Z_X + nE^Z_S) \quad (3)$$

where E_{X-S_n} ($E^Z_{X-S_n}$), E_X (E^Z_X) and E_S (E^Z_S) are electronic (zero point corrected electronic) energies of complex geometry, cyclic tripeptide and solvent molecule respectively and n is number of solvent molecules. E_{BSSE} is BSSE correction.

Using the structures complexed with solvent molecules, showing strong interactions energies, solvent assisted reaction pathways (**RRR-CyR**: **RRR-x** → **RRR-Cy-x** and **RRS-CyR**: **SRR-x** → **RRS-Cy-x** where x ≡ 2 units of DMF) for cyclization of linear tripeptides were modeled. Both the stepwise and concerted mechanisms were used to locate the transition states and intermediates. Since cyclic structures are conformationally more rigid as compared to the linear structures, the modeling of transition states (TS), intermediates (INT) and linear tripeptides was based on minimum energy structures of the products. For example, the transition state, **RRR-TS2-x-s** (see Fig. 2) was obtained by keeping a water molecule close to the carbonyl group of most stable solvent associated conformer of **RRR-Cy-x**, followed by transition state optimization. Similarly **RRR-INT-x-s** was obtained by elongation and shortening of selected bonds in **RRR-TS2-x-s** followed by energy minimization and so on. Geometry optimization was carried out at the B3LYP/6-31G(d,p) and M06 [41]/6-31G(d,p) levels of theory in gas phase. Default cut-off for convergence implemented in the Gaussian09 [42] program was used for all the calculations. The optimized geometries were further subjected to Hessian calculations. Vibrational frequencies of all geometries except TSs were found to be real and the TSs obtained were characterized by one imaginary frequency for each. Visual analysis of nuclear motion in the TS confirms the mechanism suggested in Fig. 2(b) and (c). For example, displacement of groups H, O—H(in water) and C(—N) in **RRR-TS2-x-s** and **RRR-TS-x-c** in modes of vibration with imaginary frequency indicates that they connect two minima on the potential energy surface. Such location of stationary points is desirable [43] for accurate analysis. Changes in ZPE corrected electronic energy (ΔE) and free energy (ΔG) for formation of each complex structure occurring in the pathways were calculated.

Single point energy (E_{el}) calculations on geometries in the reaction pathways, explored at B3LYP/6-31G(d,p) level of theory, were carried out using B3LYP functional and an array of

basis sets, namely, 6-311G(d,p), 6-311+G(d,p), 6-311++G(d,p), cc-pVDZ, aug-cc-pVDZ and cc-pVTZ in order to estimate the dependence of energies on the quality of basis sets used. Additionally, calculations such as M06/6-31G(d,p)//B3LYP/6-31G(d,p) and MP2/6-31G(d,p)//B3LYP/6-31G(d,p) were also carried out. Effects of electron correlation on reaction energies of the species were studied and the results for barrier heights from using the two DFT functionals compared by comparing electronic energies obtained at MP2, M06 and B3LYP levels of theory. The calculations were also carried out in the solvent, DMF, using PCM at B3LYP/6-31G(d,p) level of theory to estimate the solvent effects.

For further investigation, geometries optimized at B3LYP/6-31G(d,p) level of theory were used. Geometric analysis was carried out on all the geometries, except for intermediate and transition state geometries involved in reaction pathways. We looked for presence of stabilizing hydrogen-bonding interactions. The criteria used for recognition of interactions, A···H—D are: 2.5 Å ≤ A . . . D distance ≤3.0 Å, and 100° ≤ A···H—D bond angle ≤ 180° [33].

Counting the hydrogen bonds in the structures does not necessarily provide insights into stability [44]. IR spectra is very sensitive to the presence of H-bonds and leads to a qualitative diagnosis about the H-bonding [45]. We computed IR spectra for all the peptides in order to estimate interaction energies of the H-bonds. To compensate for the anharmonic effects, the vibrational stretching frequencies of donor groups were scaled using a scaling factor of 0.9608, as appropriate for B3LYP/6-31G(d,p) level of theory (http://cccbdb.nist.gov/vsf.asp).

Natural Bond Orbital (NBO) [46] analysis was performed in order to quantify all possible stabilizing intramolecular interactions in the species. Interactions between filled Lewis and empty non-Lewis orbitals were determined and energies of second order stabilization, $E^{(2)}$ [47], due to transfer of electron cloud from donor NBO(i) to acceptor NBO(j) were obtained using the equation

$$E^{(2)} = q_i \left[\frac{(F(i,j))^2}{E_j - E_i} \right] \quad (4)$$

where q_i is donor orbital occupancy, E_i and E_j are energies of the orbitals i, j respectively, and $F(i,j)$ is the off diagonal NBO Fock matrix element.

The topology of electron density distribution along the bond path of atoms interacting through hydrogen bonding was determined using AIMALL [48,49]. The interactions were characterized in terms of electron density, $\rho(\mathbf{r})$, Laplacian of electron density, $\nabla^2\rho(\mathbf{r})$, kinetic energy density, G($\mathbf{r}$), potential energy density, V($\mathbf{r}$) and electronic energy density H($\mathbf{r}$) at bond critical points [50].

Molecular electrostatic potential (MESP) surface [51–54] indicates the potential energy within the space occupied by the molecule. This property is sensitive to the structural changes in molecules. We analyzed the MESP surfaces of all cyclic peptides optimized in gas phase in order to gain further insights into their structural properties. The ESP contours for the cyclic tripeptides were generated using MOLDEN [55]. Using GaussView, ESP surfaces of cyclic peptides are mapped onto the corresponding electron density plots with isodensity setting of 0.0004 a.u. Isovalue of the electron density surface is defined by 0.002-electrons/bohr^3 contour of the molecular electron density. MESP mapped onto electron isodensity plots of the cyclic peptides were analyzed for electron rich, depletion and no charge regions. All quantum chemical calculations were carried out using the Gaussian09 [42] suite of programs.

3. Results and discussion

Relevant optimized structures without and with explicit solvation are shown in Fig. 3. We discuss first the energetics, and details of structure including the non-covalent interaction are discussed later. Following notation is used in subsequent discussion – **PG**: Gas Phase, **PSO**: Solvent Phase Onsager model, **PCM**: Solvent Phase PCM.

3.1. Energetic aspects

Table 1 summarizes energetics for formation of linear di, tri and cyclic tripeptides in both gas and implicit solvent phases. The absolute values of energies for all the peptides are shown in Tables S2(a) and S2(b) (supplementary information).

3.1.1. Linear dipeptides

Magnitudes of change in electronic energy (ΔE) and free energy (ΔG) for formation of **RR**, **SS** and **RS** are equal and slightly less for **SR**, optimized in **PG**. In **PSO** while formation of **RS** occurs with the lowest value of ΔE (−4.2 kcal/mol), ΔG is more favorable for **SS** (−3.2 kcal/mol). A positive contribution from entropic term ($T\Delta S$) to ΔG (see Table S2(b)) makes it a slightly favorable product. In **PCM**, magnitudes of ΔE for formation of the peptides are equal, ΔG is slightly favorable for **RS**. Overall, maximum difference in both ΔE and ΔG for formation of dipeptide is 0.5 and 0.8 kcal/mol in **PG** and 0.3 (0.1) and 0.9 (0.4) kcal/mol in **PSO** (**PCM**) respectively. The difference being less than 1 kcal/mol, we conclude that chirality has an insignificant role in linear dimerization of AEFC.

3.1.2. Linear tripeptides

As expected, the homochiral enantiomers, **RRR** and **SSS** do not differ in values for ΔE and ΔG, for formation (−17.1 and −9.2 kcal/mol respectively in gas phase (Table 1)). These are slightly larger (in magnitude) than the heterochiral tripeptides in both **PG** as well as **PSO**. In **PCM**, magnitudes of ΔE and ΔG for the peptides **SRR** and **RSS** are larger as compared to other peptides. Among hetero isomeric tripeptides, **SRR** and **RSS** are energetically favorable structures. The maximum difference in ΔE (ΔG) is 2.3 (2.3), 1.7(1.7) and 1.2(1.5) kcal/mol in **PG**, **PSO** and **PCM** respectively (Table 1). For the heterochiral species this difference is insignificant. The results show a small homo isomeric preference in the formation of linear tripeptides in gas phase and a heterochiral preference in relatively accurate implicit PCM. More accurate results from microsolvation data show a trend significantly opposite to that observed in gas phase and implicit Onsager solvent phase model (Fig. 4).

3.1.3. Cyclic tripeptides

Formation of cyclic tripeptides shows homochiral preference in both gas phase as well as solvent phase. **RRR-Cy** and **SSS-Cy** are favored more than **RRS-Cy** and **RSS-Cy** by about 1.5 (2.0) kcal/mol in terms of both ΔE and ΔG in gas phase (solvent phase). It is noticed that the decrease in electronic energy as well as free energy change is generally less for cyclic tripeptides as compared to their linear analogs. The values for gas phase are, $\Delta(\Delta E) = \Delta E_{\mathbf{RRR}} - \Delta E_{\mathbf{RRR-Cy}} = -11.4$ kcal/mol and $\Delta(\Delta G) = \Delta G_{\mathbf{RRR}} - \Delta G_{\mathbf{RRR-Cy}} = -2.7$ kcal/mol.

3.1.4. Microsolvation of tripeptides

The solvent molecules were positioned around the cyclic tripeptides such that the carbonyl oxygen of DMF molecule interacts with NH-moiety of the tripeptides via hydrogen bonding. Absolute values of E and G for the systems complexed with solvent molecules, optimized in gas phase as well as solvent phase (**PCM**) are summarized in Table S3(a). The interaction energies are shown in Table 2.

The structure, **RRR-Cy-1DMF**, shows a slightly larger interaction with solvent molecule ($E_{3-int} = -10.2$ kcal/mol) when compared to that of **RRS-Cy-1DMF** ($E_{3-int} = -9.6$ kcal/mol) in gas phase. Two conformations for each of the peptides with two solvent molecules

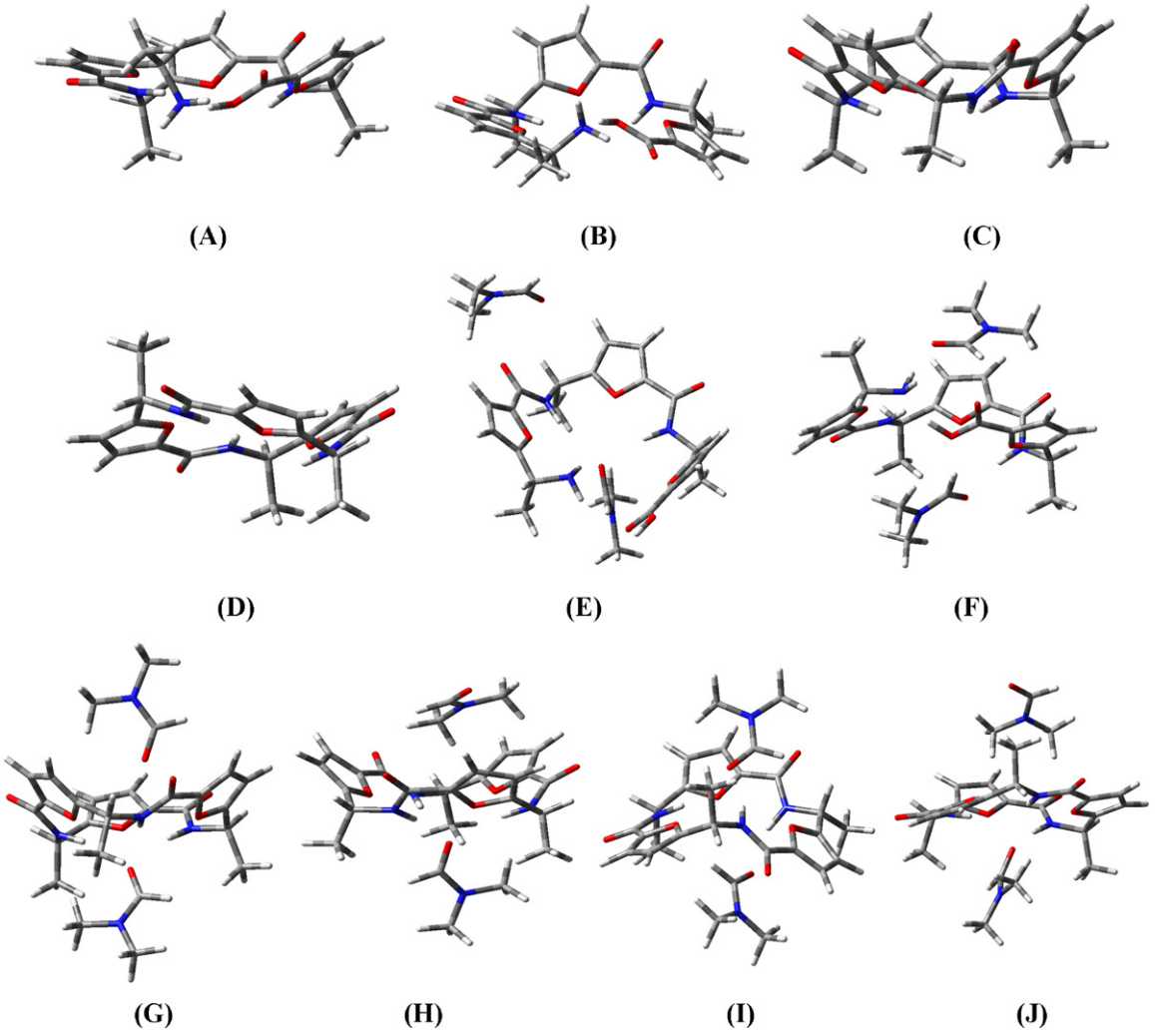

Fig. 3. Linear and cyclic tripeptides of AEFC optimized at B3LYP/6-31G(d,p) level of theory in gas phase. (A) **RRR**, (B) **SRR**, (C) **RRR-Cy**, (D) **RRS-Cy**, (E) **RRR-2DMF-s**, (F) **SRR-2DMF-s**, (G) **RRR-Cy-2DMF; Con I**, (H) **RRR-Cy-2DMF; Con II**, (I) **RRS-Cy-2DMF; Con I**, (J) **RRS-2Cy-2DMF; Con II. 'Con'** denotes 'Conformation'. In both Con I and Con II, the initial geometry for optimization is prepared by taking two solvent molecules, one above and another below the plane of cyclic tripeptides and lying on three-fold axis of rotation for the peptides.

Table 1
Change in zero point corrected electronic energy (ZPE), ΔE, and free energy, ΔG, for formation of linear di, tri and cyclic tripeptides, calculated at B3LYP/6-31G(d,p) level of theory for gas phase, **PG**, implicit solvation using Onsager reaction field model, **PSO** and **PCM**.

	PG		**PSO**		**PCM**	
Species	ΔE (kcal/mol)	ΔG (kcal/mol)	ΔE (kcal/mol)	ΔG (kcal/mol)	ΔE (kcal/mol)	ΔG (kcal/mol)
RR	−3.4	−1.9	−3.9	−2.7	−4.3	−2.5
SS	−3.4	−1.9	−4.0	−3.2	−4.3	−2.5
RS	−3.4	−2.0	−4.2	−2.3	−4.3	−2.9
SR	−2.9	−1.2	−3.9	−2.4	−4.4	−2.6
RRR	−17.1	−9.2	−19.4	−11.5	−17.5	−10.3
SSS	−17.1	−9.2	−19.4	−11.4	−17.5	−10.3
SRR	−16.4	−8.9	−18.7	−11.2	−17.9	−10.4
RSS	−16.4	−8.9	−18.7	−11.2	−17.9	−10.4
RSR	−14.8	−6.9	−18.0	−10.3	−17.0	−9.4
SRS	−15.5	−7.5	−17.8	−9.8	−16.7	−8.9
RRS	−14.9	−6.9	−18.0	−10.4	−17.1	−9.6
SSR	−14.9	−6.9	−17.7	−10.0	−17.1	−9.6
RRR-Cy	−5.7	−6.5	−9.5	−10.5	−10.6	−11.4
SSS-Cy	−5.7	−6.4	−9.5	−10.4	−10.6	−11.3
RRS-Cy	−4.3	−5.0	−7.5	−8.4	−8.5	−9.1
RSS-Cy	−4.3	−5.0	−7.5	−8.4	−8.5	−9.1

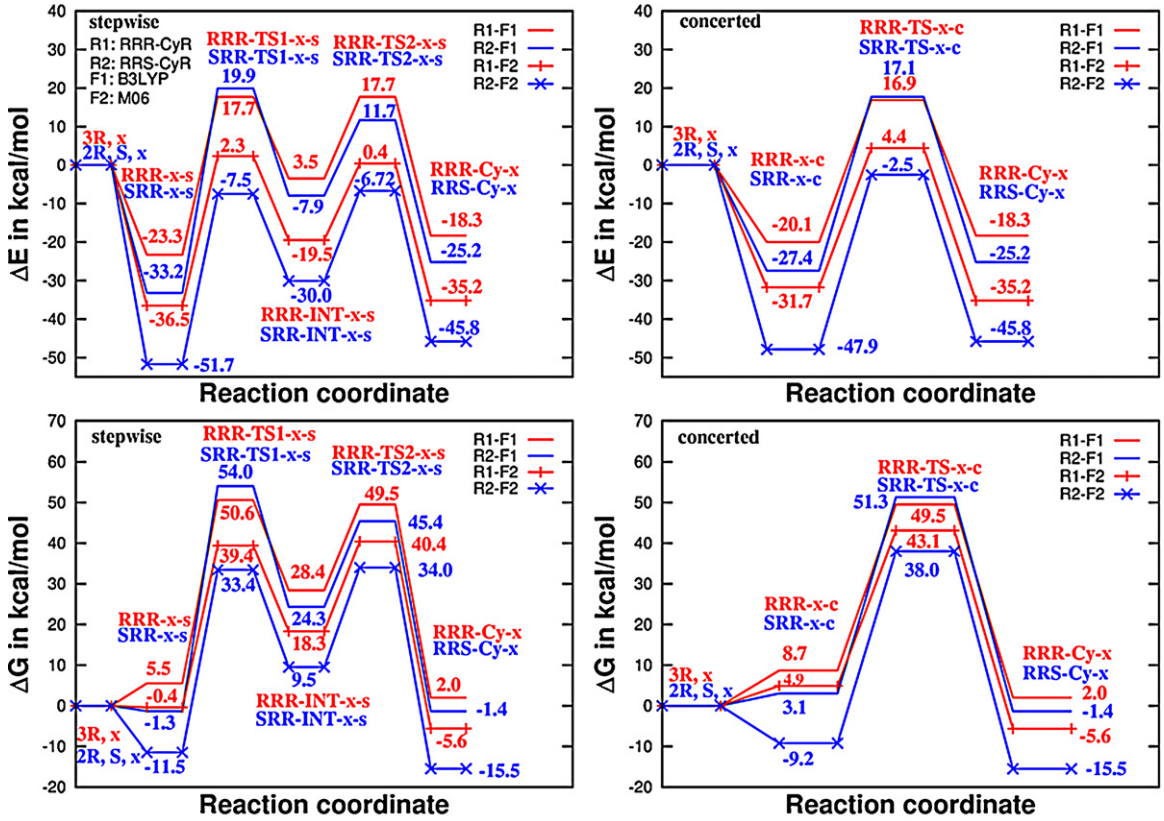

Fig. 4. Relative values of zero point corrected electronic energy (ΔE) and free energy (ΔG) of various solvated structures obtained in both the pathways of reactions, **RRR-CyR** and **RRS-CyR** calculated at B3LYP/6-31G(d,p) and M06/6-31G(d,p) levels of theory in gas phase. Each geometry in pathway is complexed with two units DMF molecules (x ≡ 2DMF). The profiles denoted by R1-F1, R1-F2 indicates pathways for reaction **RRR-CyR** explored at B3LYP/6-31G(d,p) and M06/6-31G(d,p) levels of theory respectively. Similarly, R2-F1, R2-F2 denote pathways for reaction **RRS-CyR** explored at B3LYP/6-31G(d,p) and M06/6-31G(d,p) levels of theory respectively. Data on absolute energies of reactants, critical points are shown in Table S3(b).

were studied (Table 2 and Fig. 3). Both show equal interaction energies (E_{3-int} = −12.6 kcal/mol). But **RRR-Cy-2DMF; Con I** does not lie on a local minimum. Interestingly asymmetric cyclic tripeptide, i.e., **RRS-Cy-2DMF; Con I** shows a significant interaction energy, i.e., −20.9 kcal/mol. This is a relatively stronger interaction than that shown by other complex structures. BSSE corrected electronic energies of interaction also show the same trend. The values of E_{3-int} obtained from solvent phase (**PCM**) calculations also show a similar trend, but with decreased magnitudes as compared to that in **PG**. This is an important observation, and contrary to the result observed in gas phase as well as in implicit solvent phase calculations on isolated cyclic peptides.

To further investigate this outcome, explicit solvent assisted reaction pathways leading to the cyclic tripeptides are modeled in gas phase, using only the solvated-complex structures showing stronger interaction energies, namely, **RRR-Cy-2DMF; Con II** and **RRS-Cy-2DMF; Con I**. Absolute values of ZP corrected electronic energies (E) and free energies (G) of the geometries in pathway are shown in Table S3(b). Change in zero point corrected electronic energies (ΔE) and free energies (ΔG) for formation of various structures in stepwise and concerted reaction pathways are shown in Fig. 4.

3.1.5. *Preference for heterochiral conformation*

We first discuss geometries optimized at B3LYP/6-31G(d,p) level of theory. The ΔE for formation of **SRR-2DMF-s** and **SRR-2DMF-c**, (see Figs. 2 and 3 for notation) is more favorable than that of **RRR-2DMF-s** and **RRR-2DMF-c** by 9.9 and 7.3 kcal/mol respectively. Similarly, the value for formation of heterochiral cyclic tripeptide i.e., **RRS-Cy-2DMF** is favorable over homochiral cyclic tripeptides, **RRR-Cy-2DMF** by 6.9 kcal/mol. The study shows that AEFC has a significant heterochiral preference for formation of both the linear

Table 2
Electronic energies of interaction of cyclic tripeptides, **RRR-Cy** and **RRS-Cy** complexed with solvent molecules of DMF, calculated at B3LYP/6-31G(d,p) level of theory for gas phase, **PG**, and implicit **PCM**.

Complex	**PG**		**PCM**	
	Without BSSE correction E_{1-int} (kcal/mol)	With BSSE correction E_{2-int} (kcal/mol)	With ZPE correction E_{3-int} (kcal/mol)	With ZPE correction E_{3-int} (kcal/mol)
RRR-Cy-1DMF	−11.4	−5.6	−10.2	−7.6
RRS-Cy-1DMF	−11.0	−4.6	−9.6	−6.7
RRR-Cy-2DMF; Con I	−15.5	−6.0	−12.6	−8.4
RRS-Cy-2DMF; Con I	−23.7	−11.4	−20.9	−12.7
RRR-Cy-2DMF; Con II	−14.2	−5.3	−12.6	−8.8
RRS-Cy-2DMF; Con II	−13.5	−4.0	−11.8	−7.9

and cyclic tripeptides in realistic environment. The ΔG also shows favorable formation of the heterochiral linear and cyclic peptides. In terms of change in free energy, the linear tripeptides are less stable as compared to the cyclic tripeptides. All these results are contrary to those obtained in gas phase and implicit solvent phase, **PSO**, and they show that the yield of heterochiral tripeptide is high in the explicit solvent phase.

The ΔG profile of the stepwise reaction pathway indicates that the free energy of activation for the transition state solvated-**RRR-TS1** is less than for solvated-**SRR-TS1** by 3.4 kcal/mol, while for the other transition state, TS2, it is just the opposite; the free energy of activation for solvated-**SRR-TS2-2DMF-s** is less by 4.1 kcal/mol. The activation energy difference (1.8 kcal/mol) between the two transition states in the concerted pathway is very small. It is known that B3LYP functional underestimates barrier heights due to self interaction error [56]. The M06 functional is reported to be better for calculating barrier heights and noncovalent interactions [56]. Activation energies for the reactions calculated at M06/6-31G(d,p) level of theory are relatively low. Also, a clear kinetic preference for heterochiral cyclic trimerization is observed (see Fig. 4). The free energy of activation for **SRR-TS1-2DMF-s**, **SRR-TS2-2DMF-s** and **SRR-TS-2DMF-c** is smaller than that of **RRR-TS1-2DMF-s**, **RRR-TS2-2DMF-s** and **RRR-TS-2DMF-c** by 6.0, 6.4 and 5.1 kcal/mol respectively. The observed kinetic and thermodynamic preference for heterochiral cyclic trimerization of AEFC indicates that the peptide, **RRS-Cy** is a high yield product.

Change in single point energy (denoted ΔE_{el} to distinguish from ΔE described earlier) for formation of complex geometries calculated at an array of basis sets mentioned in methodology section also substantiated the observed energetic trends. The ΔE_{el} profile for the reactions is shown in Fig. 5 (additional data in Table 3 and Tables S4(a) and (b)). The ΔE_{el} obtained from M06/6-31G(d,p)//B3LYP/6-31G(d,p) and MP2/6-31G(d,p)//B3LYP/6-31G (d,p) calculations show significantly reduced electronic energy barriers and formation energies of products when compared to that determined at B3LYP/6-31G(d,p) level of theory. The values of electronic energy of activation obtained from these two levels of theory show kinetic preference for heterochiral cyclization along both the pathways (see Table 3). The relatively larger reduction obtained using MP2 method is due to improved accuracy in the description of correlation energies and overestimation of the dispersion interaction energy [57–60] are reasons for significant reduction of the barrier heights.

Comparison of ΔE_{el} calculated at B3LYP/6-31G(d,p) level of theory in gas phase and implicit solvent phase (**PCM**) for geometries in reaction pathways is shown in Table 4 (absolute values of E are in Table S4(c)). In solvent phase, magnitudes of the electronic energy of activation increase as compared to that in gas phase. The change in electronic energy of formation for linear and cyclic peptides in the solvent phase shows preference for heterochiral cyclic trimerization.

An important conclusion from the study is that the favorable formation of heterochiral peptides is primarily caused by its interactions with solvent molecules. The effect of observed homochiral preference for the formation of **RRR-Cy** in gas phase is imperceptible in explicit solvent phase. The focus of subsequent discussion is on stable geometries of linear and cyclic tripeptides.

3.2. Structural aspects

We have investigated the geometries of peptides to locate H-bonding interactions. Below we discuss the details.

3.2.1. Linear dipeptides

Geometries of monomers and dipeptides optimized and magnitudes of parameters for associated H-bond interactions are provided in supplementary information (gas phase data in Fig. S1 and solvent phase data in Table S5).

Each dipeptide shows one H-bonding interaction, N10—H11···O6. The O···H bond distance, and angle for the interaction are 2.30 Å and 103.9° respectively in both the homochiral peptides. These are 2.31 Å, 103.8° and 2.30 Å, 104.3° in **RS** and **SR** respectively. In implicit solvent phase the parameters remain nearly same thus explaining the close values for the free energy of dipeptide formation. These interactions are further used for comparison of potential H-bonds in linear and cyclic tripeptides.

3.2.2. Linear tripeptides

Optimized geometries of **RRR** and **SRR** and corresponding solvated structures are shown in Fig. 6. Data with details for all systems are provided in the supplementary information (Fig. S2 and Table S6).

Both the peptides **RRR** and **SRR** show interactions, O26—H27···N3, N3—H1···O25, N10—H11···O6 and N18—H19···O14. Comparison of bond length (H···A) and angle parameters of corresponding interactions in the two systems reveals a marginal difference, except for the bond angle of N3—H1···O25, where it is relatively more linear in **SRR** (123.1°) as compared to that in the **RRR** (116.2°). The observations remain same in implicit solvent phase. But the peptides show significant difference when interaction with solvent molecules is considered explicitly. While **RRR-2DMF-s** shows a trifurcated intermolecular H-bonding interaction, i.e, N—H···O=C(DMF), **SRR-2DMF-s** is associated with two regular H-bonding interactions, N3—H2···O64, N18—H19···O52 where O64 and O52 are the oxygen atoms in the solvent molecules (see Fig. 6). A significant difference is that homochiral peptide shows the N—H···O interaction with only one solvent molecule, where as the heterochiral peptides interacts with both the solvent molecules, via N—H···O bonds. The bond lengths (H···A) of intermolecular interactions are relatively small in heterochiral peptide. Moreover trifurcation of the interaction might be a cause for less stability of homochiral peptides as compared to its heterochiral counterpart. While, solvated **SRR** has four intramolecular interactions, solvated **RRR** shows three such interactions. The observations substantiate favorable formation of the heterochiral linear tripeptide.

3.2.3. Cyclic tripeptides

Axial view of cyclic tripeptides **RRR-Cy** and **RRS-Cy** optimized in gas phase and the geometric parameters of H-bond interactions are shown in Fig. 7. The other two cyclic peptides are shown in Fig. S3. Details for optimized geometries in implicit solvent phase are summarized in Table S7.

While the homochiral tripeptides have a C_3 symmetric tripod bowl shaped structure, heterochiral peptides do not show this symmetry. The peptides **RRR-Cy**, **SSS-Cy** show three hydrogen bonding interactions, N2—H1···O21, N9—H10···O5 and N17—H18···O13. On the other hand, **RRS-Cy** and **RSS-Cy** have a pair of three centered hydrogen bonding interactions (see Fig. 7) and an interaction N17—H18···O13. The H-bond, N2—H1···O21 in heterochiral peptides has a larger bond distance and a smaller angle as compared to that in homochiral peptides. Magnitudes of the parameters of other two interactions are approximately equal in all the gas phase as well as implicit solvent phase structures. These are further characterized in subsequent sections.

Microsolvation of cyclic tripeptides changes geometric aspects of cyclic tripeptides **RRR-Cy** and **RRS-Cy** due to explicit interactions of solvent molecules.

Gas phase optimized geometries of **RRR-Cy-1DMF**, **RRS-Cy-1DMF** (Fig. S4) show all the intramolecular hydrogen bonding interactions that are observed in isolated cyclic structures. In addition, the carbonyl oxygen of DMF molecule forms a trifurcated

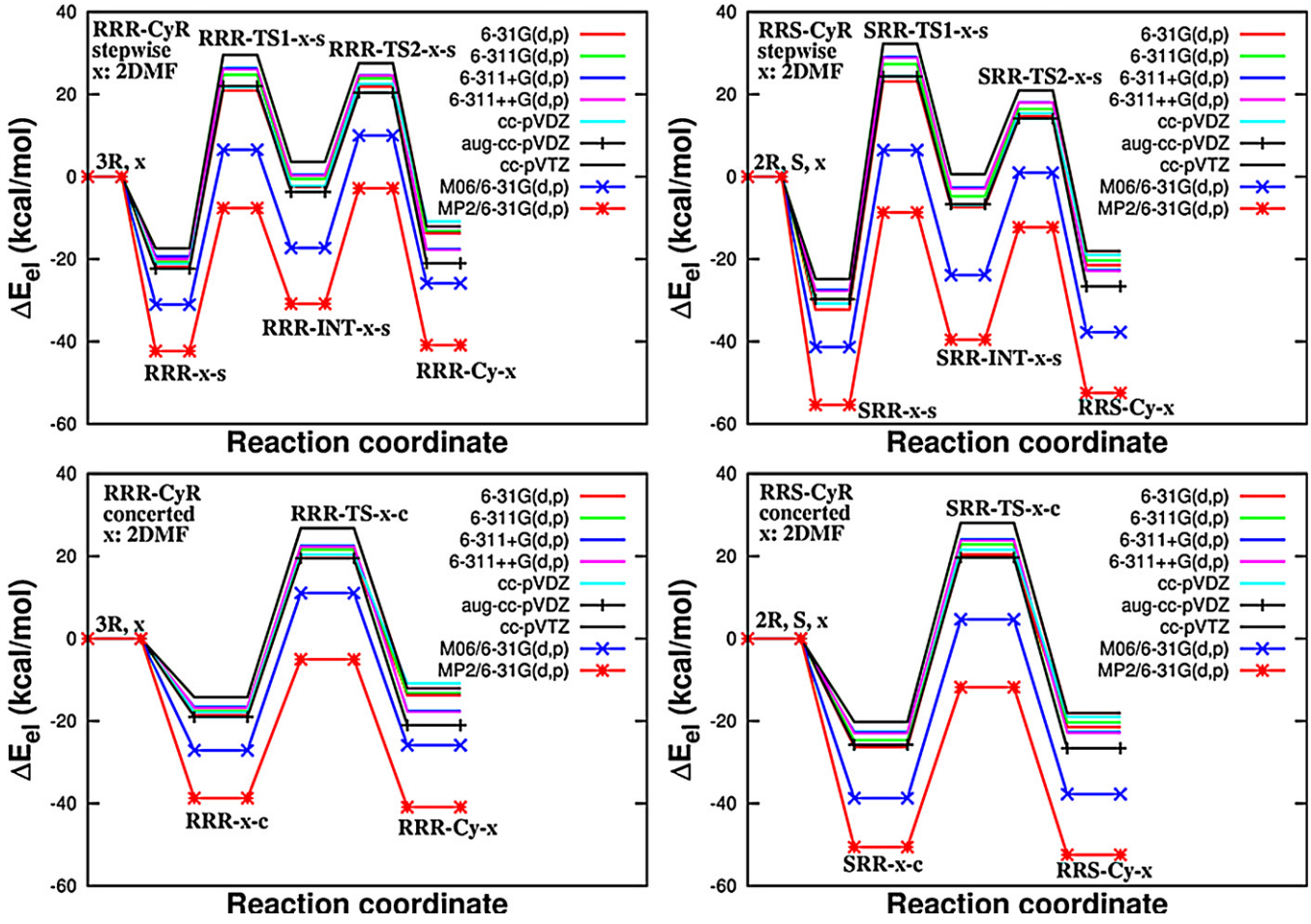

Fig. 5. Change in electronic energy (ΔE_{el}) in solvent assisted stepwise and concerted reaction pathways for reactions **RRR-CyR** and **RRS-CyR** calculated at (i) B3LYP/6-31G(d,p) [referred to as i henceforth]; (ii) B3LYP/6-311G(d,p)//i; (iii) B3LYP/6-311+G(d,p)//i; (iv) B3LYP/6-311++G(d,p)//i; (v) B3LYP/cc-pVDZ//i; (vi) B3LYP/aug-cc-pVDZ//i; (vii) B3LYP/cc-pVTZ//i; (viii) M06/6-31G(d,p)//i; and (ix) MP2/6-31G(d,p)//i levels of theory in gas phase. Data on absolute energies of reactants and critical points are shown in Tables S4(a) and S4(b).

hydrogen bonding interaction with three NH— groups of each cyclic tripeptide. Overall, the bond angles are more favorable (closer to linear) in **RRR-Cy-1DMF** as compared to in **RRS-Cy-1DMF**. The different geometric features of the H-bond interactions reflect distinct orientations of amide groups in homo and heterochiral peptides. The data agree with interaction energies for both the complexes.

The gas phase optimized geometries of **RRR-Cy-2DMF; Con I, II** and **RRS-Cy-2DMF; Con I, II** are shown in Figs. 8 and 9, respectively. The two conformations of each structure differ in the orientation of DMF molecules with respect to the solute molecule.

The structures, **RRR-Cy-2DMF; Con I, II** (Fig. 8) exhibit three intramolecular H-bonding interactions, N2—H1···O21,

Table 3
Change in electronic energy (ΔE_{el}) for formation of geometries in solvent assisted stepwise and concerted pathways of reactions, **RRR-CyR** and **RRS-CyR**, calculated at (i) B3LYP/6-31G(d,p) [referred to as i henceforth], (ii) B3LYP/6-311G(d,p)//i, (iii) B3LYP/6-311+G(d,p)//i, (iv) B3LYP/6-311++G(d,p)//i, (v) B3LYP/cc-pVDZ//i, (vi) B3LYP/aug-cc-pVDZ//i and (vii) B3LYP/cc-pVTZ//i, (viii) M06/6-31G(d,p)//i and (ix) MP2/6-31G(d,p)//i levels of theory in gas phase. All values are in kcal/mol. x ≡ 2 DMF (two units of N, N, DMF). For comparison, the values of ΔE_{el} for geometries in pathway leading to **RRS-Cy** are in given in bold font.

Structure	ΔE_{el} at								
	i	ii	iii	iv	v	vi	vii	viii	ix
RRR-x-s	−21.9	−20.6	−19.8	−20.0	−21.1	−22.3	−17.3	−31.0	−42.3
SRR-x-s	**−32.3**	**−29.7**	**−27.5**	**−27.7**	**−30.7**	**−29.8**	**−24.8**	**−41.4**	**−55.4**
RRR-TS1-x-s	20.9	24.7	26.3	26.1	21.7	22.0	29.6	6.5	−7.6
SRR-TS1-x-s	**23.1**	**27.3**	**29.1**	**28.9**	**24.4**	**24.3**	**32.3**	**6.5**	**−8.7**
RRR-INT-x-s	−2.4	−0.5	0.5	0.3	−2.3	−3.7	3.6	−17.2	−30.9
SRR-INT-x-s	**−7.4**	**−4.7**	**−2.7**	**−2.9**	**−6.9**	**−6.7**	**0.6**	**−23.8**	**−39.6**
RRR-TS2-x-s	21.9	23.9	24.6	24.5	22.5	20.4	27.6	9.9	−2.8
SRR-TS2-x-s	**14.7**	**16.4**	**18.1**	**18.0**	**15.4**	**14.1**	**20.9**	**0.9**	**−12.3**
RRR-x-c	−18.9	−17.6	−16.6	−16.8	−17.9	−19.0	−14.2	−27.1	−38.7
SRR-x-c	**−26.4**	**−24.7**	**−22.7**	**−22.9**	**−25.8**	**−25.7**	**−20.2**	**−38.7**	**−50.6**
RRR-TS-x-c	20.3	21.6	22.5	22.3	20.4	19.5	26.8	11.1	−5.0
SRR-TS-x-c	**20.4**	**22.8**	**24.1**	**23.9**	**21.6**	**19.7**	**28.1**	**4.7**	**−11.8**
RRR-Cy-x	−13.7	−13.2	−17.6	−17.8	−10.9	−21.0	−12.1	−25.9	−40.9
RRS-Cy-x	**−21.5**	**−20.3**	**−22.7**	**−22.8**	**−19.0**	**−26.6**	**−18.1**	**−37.8**	**−52.5**

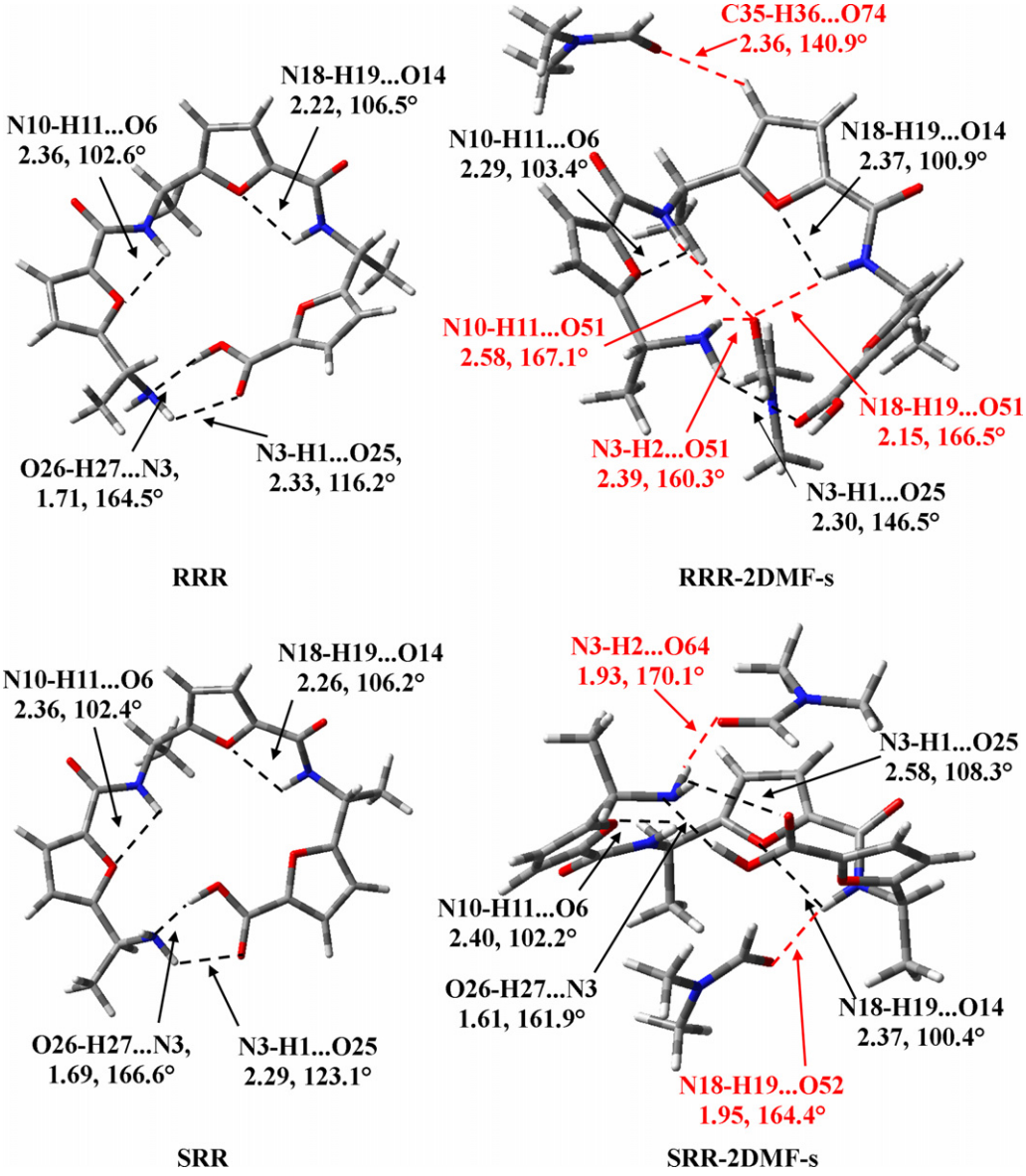

Fig. 6. Geometries of linear tripeptides, **RRR**, **SRR**, **RRR-2DMF-s** and **SRR-2DMF-s** optimized at B3LYP/6-31G(d,p) level of theory in gas phase. The dotted lines indicate potential H-bonding interactions. Atom specification of H-bonds is shown. Magnitudes of bond distance (O···H) (in Å) and bond angle are shown.

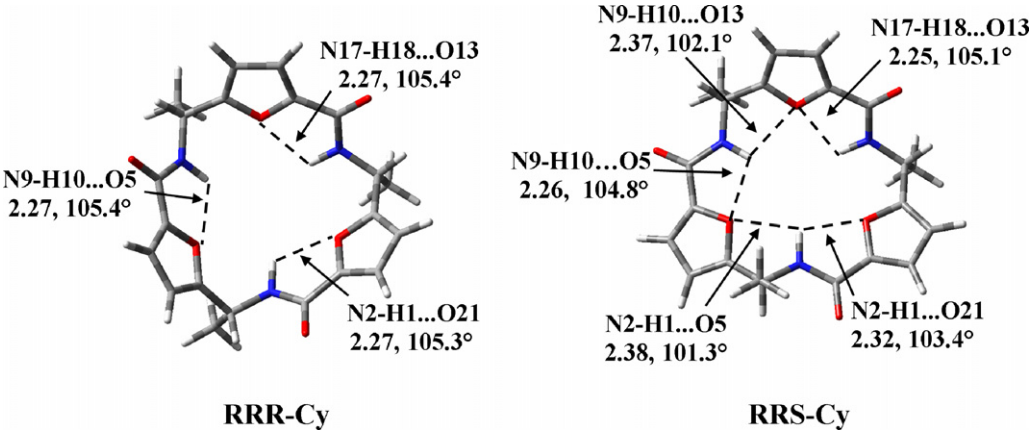

Fig. 7. Axial view of cyclic tripeptides **RRR-Cy**, **RRS-Cy** optimized at B3LYP/6-31G(d,p) level of theory in gas phase. The dotted lines indicate potential H-bonding interactions. Atom specification of H-bonds is shown. Magnitudes of bond distance (O···H) (in Å) and bond angle are shown.

Table 4
Change in electronic energy of formation, ΔE_{el}, for solvated geometries obtained in stepwise and concerted reaction pathways leading to cyclization, calculated at B3LYP/6-31G(d,p) level of theory in gas phase, **PG**, and implicit solvent phase, **PCM**. The values are in kcal/mol. **x** ≡ 2DMF (2 units of DMF molecules). Data on absolute energies of reactants and other geometries are shown in Table S4(c).

Species	ΔE_{el}		Species	ΔE_{el}	
	PG	**PCM**		**PG**	**PCM**
RRR-x-s	−21.9	−15.7	**SRR-x-s**	−32.3	−24.1
RRR-TS1-x-s	20.9	28.2	**SRR-TS1-x-s**	23.1	30.8
RRR-INT-x-s	−2.4	2.2	**SRR-INT-x-s**	−7.4	0.4
RRR-TS2-x-s	21.9	26.1	**SRR-TS2-x-s**	14.7	23.5
RRR-x-c	−18.9	−14.9	**SRR-x-c**	−26.4	−19.4
RRR-TS-x-c	20.3	26.0	**SRR-TS-x-c**	20.4	26.8
RRR-Cy-x-Con II	−13.7	−14.8	**RRS-Cy-x-Con I**	−21.5	−17.0

N9—H10···O5 and N17—H18···O13. In both the complexes, bond distance (O···H) and bond angle parameters are altered as compared to the unsolvated peptides, such that strength of these bonds decreases (Fig. 8). The conformations exhibit trifurcated intermolecular H-bonding interactions, N2—H1···O52, N9—H10···O52 and N17—H18···O52 where O52 is the oxygen atom in the solvent molecule. While bond lengths (O···H distance) of the interactions are short in **Con I**, they are more linear in **Con II** of the complex geometries. In both the conformers, oxygen atoms of the other solvent molecule, O64, do not form H-bond. However, **Con I** is not a minimum energy structure, it exhibits competent H-bonding interactions as compared to those that in minimum energy geometry, i.e., **Con II**. The parameters of H-bond interactions substantiate

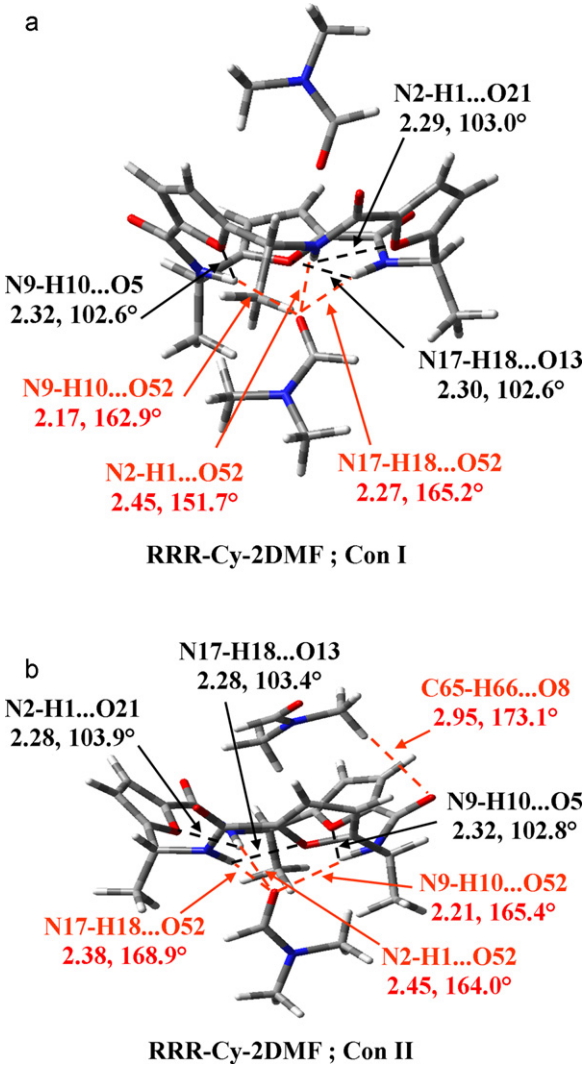

Fig. 8. Cyclic tripeptide, **RRR-Cy**, complexed with two N, N, dimethyl formamide molecules, optimized at B3LYP/6-31G(d,p) level of theory in gas phase. The dotted lines indicate potential H-bonding interactions. Atom specification of H-bonds is shown. The bonds marked with red color are intermolecular interactions. Magnitudes of bond distance (O···H) (in Å) and bond angle are shown. (For interpretation of the references to color in this figure legend, the reader is referred to the web version of the article.)

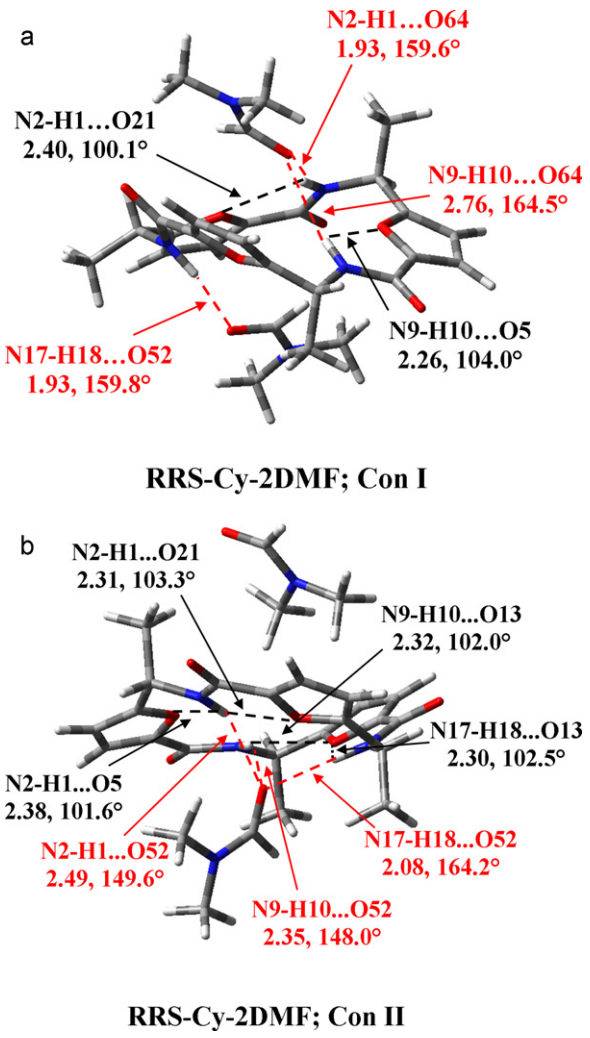

Fig. 9. Cyclic tripeptide, **RRS-Cy**, complexed with two N,N, dimethyl formamide molecules, optimized at B3LYP/6-31G(d,p) level of theory in gas phase. The dotted lines indicate potential H-bonding interactions. Atom specification of H-bonds is shown. The bonds marked with red color are intermolecular interactions. Magnitudes of bond distance (O···H) (in Å) and bond angle are shown. (For interpretation of the references to color in this figure legend, the reader is referred to the web version of the article.)

equal interactions energies (12.6 kcal/mol) shown by both the conformations.

The structure, **RRS-Cy-2DMF; Con I** shows two intramolecular H-bonding interactions, N2—H1···O21, N9—H10···O5, intermolecular interactions, N2—H1···O64, N9—H10···O64 and N17—H18···O52 (O64 and O52 are oxygen atoms in the two solvent molecules). The first two intermolecular interactions are bifurcated where O64 is common acceptor for the amide groups N2—H1 and N9—H10. Other structure **RRS-Cy-2DMF; Con II** exhibits two sets of bifurcated intramolecular interactions, (N2—H1···O5, N2—H1···O21) and (N9—H10···O13, N17—H18···O13), and a trifurcated intermolecular interaction, N2—H1···O52, N9—H10···O52 and N17—H18···O52. Geometrically, intermolecular H-bonding interactions are more favorable in **Con I** of the complex structure (see Fig. 9).

The data also indicate that the molecular structure of heterochiral peptide is more amenable to intermolecular H-bonding interactions as compared to its homochiral counterpart. This is in agreement with strong interaction energy, −20.9 kcal/mol, shown by **RRS-Cy** with solvent molecules.

3.3. IR spectra

The characteristic IR absorption frequency of stretching mode vibration of N—H and O—H bonds is extremely sensitive to hydrogen bond interaction [45]. The typical stretching frequency of free NH group occurs in the region of 3420–3550 cm^{-1} [45]. Similarly stretching frequency of free OH bond falls in the region of 3000–2500 cm^{-1}. Any red shift from this region indicates their involvement in H-bonding interaction. A general rule is that the stronger the bond, the larger is the shift [45]. A significant H-bond causes red-shifts by 100–200 cm^{-1} and weaker interactions cause smaller shifts, by less than 40 cm^{-1} [45].

We have investigated bond lengths, wavenumber and corresponding frequency shifts for NH and OH groups in all the peptides optimized in gas phase. The values for linear di, tripeptides, tripeptides complexed with solvent molecules, cyclic peptides and their complex structures are shown in Tables S8, S9(a)–(b), S10 and S11, respectively. The frequency shifts ($\Delta\nu$) of donor groups are calculated by comparing frequencies of corresponding groups in dipeptide, **RR**.

A general inference is that the interactions are generally weak as can be seen from small red shift in stretching frequency of amide groups participating in H-bonded interactions in the linear tripeptides. There are usual variations as for example, $\Delta\nu$ for N10—H11 and N18—H19 in **RRR** are slightly larger than those that in **SRR**. In case of terminal group interactions (O—H···N), the magnitudes of red shift for stretching frequency of O—H are high in **RRS/SSR**. Additional data for $\Delta\nu$ for isolated linear peptides are given in Table S9(a). The donor groups of H-bonds in the peptides complexed with solvent molecules show significant red shifts (>100 cm^{-1}). Except N10—H11, all the groups in **SRR-2DMF-s** show large red shits when compared to those that in **RRR-2DMF-s** (see Table S9(b)). The data support favorable formation of **SRR** in explicit solvent phase with optimum orientations of interacting sites for intermolecular noncovalent interactions.

Interestingly, the NH groups in cyclic peptides show smaller blue shifts. While in **RRR-Cy** the shifts are in the range of 0.1–4.8 cm^{-1} and in **RRS-Cy** they fall in the range, 9.5–20.6 cm^{-1}. The trend for **SSS-Cy** and **RSS-Cy** is similar to that for **RRR-Cy** and **RRS-Cy** respectively. This substantiates earlier observation that cyclic peptides are less stable as compared to their linear analogs in gas phase. Magnitudes of blue shift in homochiral cyclic peptide are less than that in heterochiral peptide. All these results are reversed when we study explicitly solvated systems.

The NH groups in all cyclic peptides complexed with solvent molecules show significant red shifts (see Table S11). Among all the complex structures, donor groups, N17—H18 and N2—H1 in **RRS-Cy-2DMF; Con I** show larger red shifts around 208.2 and 212.9 cm^{-1} respectively. This is in consonance with the significant interaction of the solvated structure with solvent molecules and larger magnitudes of ΔE and ΔG.

3.4. NBO and AIM analyses

Tables S12–S15 summarize the results of NBO analysis for dipeptides, linear and cyclic tripeptides. The stabilization energy $E^{(2)}$ of interactions observed in all geometries agree well with the geometrical parameters and further substantiate the conclusions obtained from energetics, geometric and IR spectra analyses. Particularly, the energies of intermolecular H-bonding interactions in **SRR-2DMF-s** and **RRS-Cy-2DMF; Con I** are significantly large (see Tables S13(b) and S15(b)).

The results of AIM analysis for gas phase optimized linear tripeptides without and with solvent molecules, cyclic tripeptides and their solvated geometries are shown in Tables, S16(a), (b), S17 and S18 respectively. All the H-bond interactions in the peptides are associated with a positive value of $\nabla^2\rho_c(\mathbf{r})$, indicating depletion of electron charge along the bond. This also indicates that the interactions are electrostatic in nature. The electronic energy density, H(**r**), is the sum of G(**r**) and V(**r**) [61]. Accumulation of charge at bond critical point, **r**, is stabilizing, if H(**r**) <0 and destabilizing, if (H(**r**) >0 [62].

The interaction, O26-H27...N3 is stronger than other existing interactions in each isolated linear tripeptide as per NBO data. The value of H(**r**) for this interaction is negative in **RRR** (−0.007 a.u.) and slightly positive in other isolated linear tripeptides (0.005 a.u.). Accumulation of charge results in stability of the solvated linear peptide, **SRR-2DMF-s**, can be seen from negative H(**r**) value for the interaction, N3—H2···O64.

The value of H(**r**) for all the interactions in each cyclic peptide is 0.003 a.u. The values are close to zero in all the stable solvated structures indicating that the cyclic peptides are mostly stabilized by intermolecular H-bonding interactions with solvent molecules.

3.5. Molecular electrostatic potential (MESP) and electron density plots

Molecular electrostatic potential (MESP) and electron density plots for all the cyclic tripeptides optimized in gas phase are generated to further substantiate the presence of intramolecular H-bond interactions and other structural features discussed above. The MESP plots are generated in the plane of three nitrogen atoms.

Figs. S5 and S6 in supporting information show MESP surfaces of homo and heterochiral peptides respectively. Contours, red in color indicate negative potential and in blue implies positive potential regions. Red contours enclosed in both homo and heterochiral cyclic tripeptides are due to the lone pair electrons of the furan oxygen atoms. The hydrogen atoms of —NH group are associated with blue colored contours, which indicate a positive potential regions. Presence of the red and blue colored contours adjacent to each other is an evidence for presence of intramolecular H-bonding interactions.

Plots of Electrostatic potential (ESP) mapped onto the electron density surfaces of molecules (Fig. S7) showing gradient of electron charge distribution with different regions of electron depletion, no charge and negative charge, exhibit distinct features arising from difference in orientation of NH-groups in the homo and heterochiral peptides. While only one face of homochiral peptides interacts with a nucleophile due to its symmetric tripod bowl shaped structure, both the faces of heterochiral peptide can interact with the

nucleophile as a result of asymmetry in its structure. It supports the strong interaction energy shown by the heterochiral peptide with solvent molecule.

4. Conclusion

We have reported theoretical insights into preferential heterochiral cyclic trimerization of 5-(aminoethyl)-2-furancarboxylic acid in explicit solvent phase. While in gas phase the formation of linear dipeptides does not show significant chiral preference, linear and cyclic tripeptides show a small homochiral preference, in explicit solvent phase the homochiral preference is imperceptible and heterochiral cyclic peptide shows larger interaction energy with solvent molecules. The solvent assisted reaction pathway leading to cyclic tripeptide from its linear analog shows significant change in free energy of formation for heterochiral linear and cyclic tripeptides, which further indicates yield of **RRS-Cy** is larger than that of **RRR-Cy**. Free energy of activation data for both the pathways calculated at M06/6-31G(d,p) level show clear kinetic preference for heterochiral cyclic tripeptide. The heterochiral cyclic tripeptide is a stable thermodynamic and kinetic product. Geometric analysis of intermolecular H-bonding interactions in structures complexed with solvent molecules supports the inferences from energetics of formation of the peptides. A further justification for the strength of stabilizing H-bonding interactions is given using computed IR spectra data, NBO and AIM analyses. Electron isodensity plots mapped with molecular electrostatic potential surfaces generated for the cyclic tripeptides **RRR-Cy** and **RRS-Cy** show that while both the faces of heterochiral cyclic tripeptide can interact strongly with solvent molecules, a homochiral cyclic peptide interacts from only one face. This gives rise to greater stability of the heterochiral cyclic product.

Our studies show clearly that gas phase or implicit solvent phase data for the linear and cyclic tripeptides formed by AEFC are inadequate in explaining realistic situations. Calculations with explicit solvation, even if with a few solvent molecules only are necessary to substantiate experimental observations. The study concludes that ability of the cyclic tripeptides to form strong noncovalent interactions increases with conversion of stereochemistry at one of its chiral center from homo to heterochiral conformation. The resulting change in molecular symmetry facilitates the interacting sites to reorient such that the peptide can interact with a nucleophile from both the faces.

Acknowledgements

We thank Department of Science and Technology, New Delhi, Government of India for financial support (SR/S1/OC-01/2007). We also thank Dr. Deva Priyakumar and Dr. Prabhakar Bhimalapuram for useful discussion. We thank the referees for suggesting calculations using M06 functional.

Appendix A. Supplementary data

Supplementary data associated with this article can be found, in the online version, at doi: http://dx.doi.org/10.1016/j.jmgm.2012.05.010.

References

[1] H. Kessler, Conformation and biological activity of cyclic peptides, Angewandte Chemie International Edition In English 21 (1982) 512–523.
[2] R.J. Brea, M. Amorín, L. Castedo, J.R. Granja, Methyl-bolcked dimeric α,γ-peptide nanotube segments: formation of a peptide heterodimer through backbone-backbone interactions, Angewandte Chemie International Edition 44 (2005) 5710–5713.
[3] K. Choi, A.D. Hamilton, Rigid macrocyclic triamides as anion receptors: anion-dependent binding stoichiometries and ^{1}H chemical shift changes, Journal of the American Chemical Society 125 (2003) 10241–10249.
[4] G.R.L. Cousins, R.L.E. Furlan, Y.-F. Ng, J.E. Redman, J.K.M. Sanders, Identification and isolation of a receptor for N-methyl alkylammonium salts: molecular amplification in a pseudo-peptide dynamic combinatorial library, Angewandte Chemie International Edition 40 (2001) 423.
[5] S. Kubik, R. Goddard, Fine tuning of the cation affinity of artificial receptors based on cyclic peptides by intramolecular conformational control, European Journal of Organic Chemistry (2001) 311–322.
[6] T.K. Chakraborty, S. Tapadar, T.V. Raju, J. Annapurna, H. Singh, Cyclic trimers of chiral furan amino acids, Synlett 14 (2004) 2484–2488.
[7] T.K. Chakraborty, S. Roy, D. Koley, S.K. Dutta, A.C. Kunwar, Conformational analysis of some C_2-symmetric cyclic peptides containing tetrahydrofuran amino acids, Journal of Organic Chemistry 71 (2006) 6240–6243.
[8] T.K. Chakraborty, S. Tapadar, S.K. Kumar, Cyclic trimer of 5-(aminomethyl)-2-furancarboxylic acid as a novel synthetic receptor for carboxylate recognition, Tetrahedron Letters 43 (2002) 1317–1320.
[9] S. Kubik, Amino acid containing anion receptors, Chemical Society Reviews 38 (2009) 585–605.
[10] S.O. Kang, R.A. Begum, K. Bowman-James, Amide-based ligands for anion coordination, Angewandte Chemie International Edition 45 (2006) 7882–7894.
[11] T. Gunnlaugsson, M. Glynn, G.M. Tocci, P.E. Kruger, F.M. Pfeffer, Anion recognition and sensing in organic and aqueous media using luminescent and colorimetric sensors, Coordination Chemistry Reviews 250 (2006) 3094–3117.
[12] P.A. Gale, Structural and molecular recognition studies with acyclic anion receptors, Accounts of Chemical Research 39 (2006) 465–475.
[13] A. Bianchi, K. Bowman-James, E. Garcia-España, Supramolecular Chemistry of Anions, Wiley-VCH, New York, 1997.
[14] G.V.M. Sharma, V. Manohar, S.K. Dutta, B. Sridhar, V.S. Ramesh, K. Ragampeta, C. Ajit, Self-assembling cyclic tetrapeptide from alternating C-linked carbo-β-amino acid [(S)-β-Caa] and α-aminoxy acid [(R)-Ama]: a selective chloride ion receptor, Journal of Organic Chemistry 75 (2010) 1087–1094.
[15] J.M. Berg, Zinc finger domains: from predictions to design, Accounts of Chemical Research 28 (1995) 14–19.
[16] L. Molina, E. Moreno-Clavijo, A.J. Moreno-Vargas, A.T. Carmona, I. Robina, Synthesis of a C_3-symmetric furyl-cyclopeptide platform with anion recognition properties, European Journal of Organic Chemistry (2010) 4049–4055.
[17] T. Agarwal, S. Roy, T.K. Chakraborty, S. Maiti, Furan based cyclic homo-oligopeptides bind G-quadruplex selectively and repress c-MYC transcription, Bioorganic and Medicinal Chemistry Letters 20 (2010) 4346–4349.
[18] T. Agarwal, S. Roy, T.K. Chakraborty, S. Maiti, Selective targeting of G-Quadruplex using furan-based cyclic homooligopeptides: effect on c-MYC expression, Biochemistry 49 (2010) 8388–8397.
[19] K. Thirumoorthy, N. Nandi, *Ab initio* study of chiral discrimination in alanine, Current Science 92 (2007) 75–80.
[20] N. Nandi, D. Vollhardt, The effect of molecular chirality on the morphology of biomimetic monolayer, Chemical Reviews 103 (2003) 4033–4075.
[21] T. Oie, G.H. Loew, S.K. Burt, J.S. Binkley, R.D. MacElroy, Quantum chemical studies of a model for peptide bond formation: formation of formamide and water from ammonia and formic acid, Journal of the American Chemical Society 104 (1982) 6169–6174.
[22] J.H. Jensen, K.K. Baldridge, M.S. Gordon, Uncatalyzed peptide bond formation in the gas phase, Journal of Physical Chemistry 96 (1992) 8340–8351.
[23] J.P. Krug, P.L.A. Popelier, R.F.W. Bader, Theoretical study of neutral and of acid and base-promoted hydrolysis of formamide, Journal of Physical Chemistry 96 (1992) 7604–7616.
[24] S. Antonczak, M.F. Ruiz-Lopez, J.L. Rivail, Ab initio analysis of water-assisted reaction mechanisms in amide hydrolysis, Journal of the American Chemical Society 116 (1994) 3912–3921.
[25] I.I. Roy Dennington, K. Todd, J. Millam, K. Eppinnett, W. Lee Hovell, G. Ray, GaussView 3.09, Semichem, Inc., Shawnee Mission, KS, 2003.
[26] W.J. Hehre, L. Radom, P.v.R. Schleyer, J.A. Pople, Ab Initio Molecular Orbital Theory, Wiley-Interscience, New York, 1986.
[27] Sybyl version7.2, c.o. http://www.tripos.com
[28] S. Gaurrand, S. Desjardins, C. Meyer, P. Bonnet, J.-M. Argoullon, H. Oulyadi, J. Guillemont, Conformational analysis of r207910, a new drug candidate for the treatment of tuberculosis, by a combined NMR and molecular modeling approach, Chemical Biology & Drug Design 68 (2006) 77–84.
[29] A.D. Becke, Density-functional exchange-energy approximation with correct asymptotic behavior, Physical Review A 38 (1988) 3098–3100.
[30] C. Lee, W. Yang, R.G. Parr, Development of the Colle-Salvetti correlation-energy formula into a functional of the electron density, Physical Review B 37 (1988) 785–789.
[31] A.D. Becke, Density-functional thermochemistry. III. The role of exact exchange, Journal of Chemical Physics 98 (1993) 5648–5652.
[32] W. Kohn, A.D. Becke, R.G. Parr, Density functional theory of electronic structure, Journal of Physical Chemistry 100 (1996) 12974–12980.
[33] H. Singh, K. Arora, S. Tapadar, T.K. Chakraborty, Preferential polymerization 5-(aminomethyl)-2-furancarboxylic acid (AMFC) into a cyclic tripeptide, Journal of Theoretical and Computational Chemistry 3 (2004) 555–566.
[34] M. Sharma, P. Kumar, H. Singh, T.K. Chakraborty, Preferential cyclotrimerization of 5-(aminomethyl)-2-furancarboxylic acid (AMFC): electrostatic and orbital interactions studies, Journal of Molecular Structure: THEOCHEM 764 (2006) 109–115.

[35] M.W. Wong, M.J. Frisch, K.B. Wiberg, Solvent effects. 1. The mediation of electrostatic effects by solvents, Journal of the American Chemical Society 113 (1991) 4776–4782.
[36] M.W. Wong, K.B. Wiberg, M.J. Frisch, Solvent effects. 2. Medium effect on the structure, energy, charge density, and vibrational frequencies of sulfamic acid, Journal of the American Chemical Society 114 (1993) 523–529.
[37] M.W. Wong, K.B. Wiberg, M.J. Frisch, Hartree-Fock second derivatives and electric field properties in a solvent reaction field: Theory and application, Journal of Chemical Physics 95 (1991) 8991–8998.
[38] J. Tomasi, M. Persico, Molecular interactions in solution: an overview of methods based on continuous distributions of the solvent, Chemical Reviews 94 (1994) 2027–2094.
[39] R. Bonaccorsi, P. Palla, J. Tomasi, Conformational energy of glycine in aqueous solutions and relative stability of the zwitterionic and neutral forms. An ab initio study, Journal of the American Chemical Society 106 (1984) 1945–1950.
[40] A.K. Rappe, C.J. Casewit, K.S. Colwell, W.A. Goddard III, W.M. Skiff, UFF, a full periodic table force field for molecular mechanics and molecular dynamics simulations, Journal of the American Chemical Society 114 (1992) 10025–10035.
[41] Y. Zhao, D.G. Truhlar, The M06 suite of density functionals for main group thermochemistry, thermochemical kinetics, noncovalent interactions, excited states, and transition elements: two new functionals and systematic testing of four M06-class functionals and 12 other functionals, Theoretical Chemistry Accounts 120 (2008) 215–241.
[42] M.J. Frisch, G.W. Trucks, H.B. Schlegel, G.E. Scuseria, M.A. Robb, J.R. Cheeseman, G. Scalmani, V. Barone, B. Mennucci, G.A. Petersson, H. Nakatsuji, M. Caricato, X. Li, H.P. Hratchian, A.F. Izmaylov, J. Bloino, G. Zheng, J.L. Sonnenberg, M. Hada, M. Ehara, K. Toyota, R. Fukuda, J. Hasegawa, M. Ishida, T. Nakajima, Y. Honda, O. Kitao, H. Nakai, T. Vreven, J.A. Montgomery, Jr., J.E. Peralta, F. Ogliaro, M. Bearpark, J.J. Heyd, E. Brothers, K.N. Kudin, V.N. Staroverov, T. Keith, R. Kobayashi, J. Normand, K. Raghavachari, A. Rendell, J.C. Burant, S.S. Iyengar, J. Tomasi, M. Cossi, N. Rega, J.M. Millam, M. Klene, J.E. Knox, J.B. Cross, V. Bakken, C. Adamo, J. Jaramillo, R. Gomperts, R.E. Stratmann, O. Yazyev, A.J. Austin, R. Cammi, C. Pomelli, J.W. Ochterski, R.L. Martin, K. Morokuma, V.G. Zakrzewski, G.A. Voth, P. Salvador, J.J. Dannenberg, S. Dapprich, A.D. Daniels, O. Farkas, J.B. Foresman, J.V. Ortiz, J. Cioslowski, D.J. Fox, Gaussian, Inc., Wallingford CT, 2010.
[43] L. Gorb, A. Asensio, I. Tuñón, M.F. Ruiz-López, The mechanism of formamide hydrolysis in water from ab initio calculations and simulations, Chemistry – A European Journal 11 (2005) 6743–6753.
[44] R.R. Gardner, S.H. Gellman, Evaluation of the conformation-directing effects of secondary hydrogen-bonding interactions in flexible tetrapeptide analogues, Journal of the American Chemical Society 117 (1995) 10411–10412.
[45] W. Chin, M. Mons, J.-P. Dognon, F. Piuzzi, B. Tardivel, I. Dimicoli, Competition betwwen local conformational preferences and sceondary structures in gas-phase model tripeptides as revealed by laset spectroscopy and theoretical chemistry, Physical Chemistry Chemical Physics 6 (2004) 2700–2709.
[46] A.E. Read, R.B. Weinstock, F. Weinhold, Natural population analysis, Journal of Chemical Physics 83 (1985) 735–746.
[47] F. Weinhold, C.R. Landis, Natural bond orbitals and extensions of localized bonding concepts, Chemistry Education Research and Practice in Europe 2 (2001) 91–104.
[48] A.K. Todd, AIMALL (Version 09.11.08), 2009.
[49] R.F.W. Bader, Atoms in Molecules, A Quantum Theory, Clarendon Press, Oxford, 1994.
[50] G.V. Gibbs, M.A. Spackman, D. Jayatilika, K.M. Rosso, D.F. Cox, Bond Length and local energy density property connections for non-transition-metal oxide-bonded interactions, Journal of Physical Chemistry A 110 (2006) 12259–12266.
[51] R.F.W. Bader, W.H. Henneker, P.E. Cade, Molecular charge distributions and chemical binding, Journal of Chemical Physics 46 (1967) 3341–3363.
[52] P. Sjoberg, P. Politzer, Use of the electrostatic potential at the molecular surface to interpret and predict nucleophilic processes, Journal of Physical Chemistry 94 (1990) 3959–3961.
[53] J.S. Murray, P. Lane, T. Brinck, P. Politzer, P. Sjoberg, Electrostatic potentials on the molecular surfaces of cyclic ureides, Journal of Physical Chemistry 95 (1991) 844–848.
[54] C.F. Matta, R.J. Gillespie, Understanding and interpreting molecular electron density distributions, Journal of Chemical Education 79 (2002) 1141–1152.
[55] G. Schaftenaar, J.H. Noordik, Molden: a pre-and post-processing program for molecular and electronic structures, Journal of Computer-Aided Molecular Design 14 (2000) 123–134.
[56] Y. Zhao, D.F. Truhlar, Density functionals with broad applicability in chemistry, Accounts of Chemical Research 41 (2008) 157–167.
[57] F. Jensen, Introduction to Computational Chemistry, second ed., John Wiley & Sons Ltd., England, 2007.
[58] W. Koch, M.C. Holthausen, A Chemist's Guide to Density Functional Theory, Wiley-VCH, 2001.
[59] P. Jurečka, J. Šponer, J. Černý, P. Hobza, Benchmark database of accurate (MP2 and CCSD(T) complete basis set limit) interaction energies of small model complexes, DNA base pairs, and amino acid pairs, Physical Chemistry Chemical Physics 8 (2006) 1985–1993.
[60] S.M. Cybulski, M.L. Lytle, The origin of deficiency of the supermolecule second-order Møller-Plesset approach for evaluating interaction energies, Journal of Chemical Physics 127 (2007) 141102–141105.
[61] D. Cremer, E. Kraka, Chemical bonds without bonding electron density-Does the difference electron-density analysis suffice for a description of the chemical bond? Angewandte Chemie International Edition In English 23 (1984) 627–628.
[62] A.H. Pakiari, Z. Jamshidi, Interaction of amino acids with gold and silver clusters, Journal of Physical Chemistry A 111 (2007) 4391–4396.